Met. Mater. Int., Vol. 20, No. 5 (2014), pp. 893~898
doi: 10.1007/s12540-014-5014-x

Extended Strain Hardening by a Sequential Operation of Twinning Induced Plasticity and Transformation Induced Plasticity in a Low Ni Duplex Stainless Steel

Jeom Yong Choi[1], Si Woo Hwang[2], Min Chul Ha[2], and Kyung-Tae Park[2,*]

[1]POSCO Technical Research Lab., STS Product Group, Pohang 790-785, Korea
[2]Hanbat National University, Dept. of Mater. Sci. & Eng., Daejeon 305-719, Korea

(received date: 30 September 2013 / accepted date: 27 December 2013)

Extended strain hardening was realized by a sequential operation of twinning induced plasticity (TWIP) followed by transformation induced plasticity (TRIP) in a Fe-20Cr-3Mn-2Cu-1Ni-1Si-0.2N duplex stainless steel (DSS). As a result, the present DSS exhibited an excellent combination of strength - ductility of 900 MPa which was 75% superior to that of conventional DSSs. The deformed microstructures of the present DSS revealed that strain induced martensite (SIM) causing TRIP primarily nucleated at intersections of mechanical twins without formation of ε martensite which is an intermediate phase during SIM transformation. In addition, the sequential operation of TWIP-TRIP enables strain hardening to be extended to higher strains compared to the operation of TWIP alone.

Keywords: metals, deformation, microstructure, transmission electron microscopy, tensile properties

1. INTRODUCTION

Duplex stainless steels (DSSs) consisting of austenite and ferrite generally exhibit better mechanical properties and corrosion resistance than single-phase stainless steels [1,2]. As with other structural metallic materials, recent development of advanced DSSs has pursued lean alloying and enhanced mechanical properties concomitantly. Control of austenite stability is considered to be one of the key strategies for two main reasons. First, the overall deformation of the DSS is more influenced by deformation of austenite, in spite of the co-presence of a considerable amount of ferrite. Second, the deformation mode of austenite strongly depends on the austenite stability. As the austenite stability decreases, the deformation modes which show extensive strain hardening operate more easily, for example, transformation induced plasticity (TRIP) and twinning induced plasticity (TWIP) [3,4]. The austenite in conventional DSS is stable mainly due to a high amount of Ni, which is a strong austenite stabilizer. Reduction of Ni makes austenite less stable and then TRIP or TWIP occurs easily. Of course, lean alloying of Ni is also cost-effective. By this strategy, low Ni TRIP [5-9] or TWIP [10] aided DSSs have been recently introduced. While conventional DSSs usually exhibit 600-800 MPa tensile strength and 30-50% elongation-to-failure, those of TRIP or TWIP aided DSSs are close to 1 GPa and over 60%, respectively.

In general, strain induced martensite (SIM) causing TRIP is known to nucleate primarily at intersections of shear bands or ε martensite bands at austenite grain interiors. However, it has often been reported that SIM nucleation is associated with mechanical twins in austenitic steels. Mangonon and Thomas [11] observed SIM nucleation at intersections of ε martensite and mechanical twins in tensile-tested 304 stainless steel. Moreover, in-grain SIM nucleation at intersections of mechanical twins was recently reported in severely deformed austenitic steels: for example, a high nitrogen austenitic stainless steel impact-tested at cryogenic temperatures [12], an ultralow carbon austenitic stainless steel severely-deformed by equal channel angular pressing [13], wire-drawn 304 stainless steel [14], a cup-drawn Mn-based austenitic TWIP steel [15], etc.

Extensive and intensive studies have been reported on the strain hardening behavior, either by TRIP, in which SIM transformation is associated with ε martensite band intersections, or by TWIP without SIM formation. However, in spite of the aforementioned microstructural evidences of SIM formation at mechanical twin intersections [11-15], little information is at present available on the strain hardening characteristic induced by SIM formation at mechanical twin intersections. When SIM formation is associated with mechanical twins, strain hardening of austenite can be extended to higher strains by a sequential operation of TWIP followed by TRIP. That is,

*Corresponding author: ktpark@hanbat.ac.kr

TWIP dominates deformation at low strains assuring substantial elongation with moderate strain hardening, and then extra strengthening and ductility can be expected from TRIP at high strains.

In this study, a DSS of Fe-20Cr-3Mn-2Cu-1Ni-1Si-0.23N-0.05C (hereafter, in wt%) was tensile-tested at room temperature and the evolution of deformed microstructure at various strains was observed, to examine the possibility of developing an advanced low Ni DSS with improved mechanical properties, by the synergetic effects of TWIP and TRIP in their sequential manner of operation. For the purpose of comparison, the strain hardening behavior of the present DSS was compared to that of TWIP aided DSS [10] which was governed by TWIP alone in the entire strain range.

2. EXPERIMENTAL PROCEDURE

The DSS (20.10Cr, 2.90Mn, 2.04Cu, 1.01Ni, 0.99Si 0.23N, 0.05C and Fe balance (in wt%)) was supplied in the form of 3.5 mm thick hot-rolled plates. The hot-rolled plates were fully annealed (1373 K for 30 min) and cold rolled to 1.3 mm. The cold rolled plates were again annealed at 1373 K for 5 min, and then water-quenched. The phase fraction was measured from at least 5 or more optical micrographs (x200) by using an image analyzer: the Murakami etchant was used to delineate austenite and ferrite. The grain size of the constituent phases was measured from electron backscattered diffraction (EBSD) using a Helios nanolab^{TM} 600 with the acceleration voltage of 20 kV (a scanning area of 145 × 105 μm^2, a step size of 200 nm) after electropolishing. Element partitioning in austenite and ferrite was examined by an electron probe micro-analyzer (EPMA, JXA-8530F) over a scanning area of 10,000 μm^2 of the samples taken from the quenched plates, under an acceleration voltage of 15 kV. Room temperature tensile tests were performed on the samples (the gage section of 25.4 mm × 6 mm × 1 mm) machined from the water-quenched plates using a universal testing machine (INSTRON model 4484) at the initial strain rate of 10^{-3} s^{-1}: the sample surface was mechanically polished and the tensile axis was parallel to the rolling direction. Some tests were interrupted at predetermined strains in order to observe the microstructures developed at different strains. The deformed microstructures were observed by using a transmission electron microscope (TEM, JEOL 3011) operating at 300 kV. The samples for TEM observation were taken from the center of the gage section of the tensile specimens, and thin foils were prepared by a twin-jet polishing technique (Struers Tenupol-5) by using a mixture of 10% perchloric acid and 90% ethanol with an applied potential of 25 V.

3. RESULTS AND DISCUSSION

Figure 1 shows a representative EBSD phase map of the present DSS in the as-quenched state. Ferrite (the red patches) was embedded into the austenite matrix (the green patches) in the form of contiguous bands along the rolling direction. The austenite and ferrite grain sizes were 4.9 ± 1.6 μm and 10.0 ± 2.7 μm, respectively, and the austenite fraction was ~0.73. The stress - strain curves of the present DSS are shown in Fig. 2a (engineering) and Fig. 2b (true). For the purpose of comparison, the tensile curves of the TWIP aided DSS are superimposed in these figures. The tensile data of the TWIP aided DSS (19.95Cr, 3.00Mn, 2.02Cu, 1.95Ni, 1.99Si, 0.22N, 0.05C, and Fe balance) were taken from Ref. [10] which the present authors recently reported.

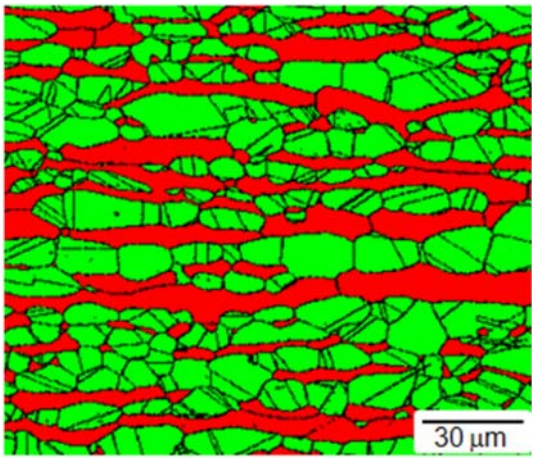

Fig. 1. A representative EBSD phase map of the present DSS annealed at 1373 K for 5 min followed by water quenching.

For the TWIP aided DSS: (a) the same heat treatments and tensile tests as the present DSS were performed; (b) the grain sizes of the constituent phases were comparable to those of the present DSS but the austenite fraction was slightly lower, as shown in Table 1; and (c) plastic deformation was entirely dominated by TWIP. The present DSS exhibited higher tensile strength and elongation than the TWIP aided DSS: the average tensile properties from three runs are shown in Table 1.

As seen in Fig. 2b, the present DSS revealed additional strengthening at high strains while the TWIP aided DSS exhibited almost linear strain hardening. In order to compare the strain hardening behavior of the two DSSs, the strain hardening rate, - normalized to the stress ($\Theta = (d\sigma/d\varepsilon)/\sigma$ where σ is the true stress and ε is the true strain) was plotted against the true strain in Fig. 2c. The present DSS exhibited two stationary points in the Θ - ε plot: the min Θ at $\varepsilon \sim 0.24$ and the peak Θ at $\varepsilon \sim 0.38$. The increase of Θ between the two stationary points is definitely attributed to strain hardening of the austenite because the strain hardening rate of ferrite continuously decreases with strain by wavy glide and dislocation cell formation, for example, as in Fig. 5d in ref. [8] and Fig. 5 in ref. [9].

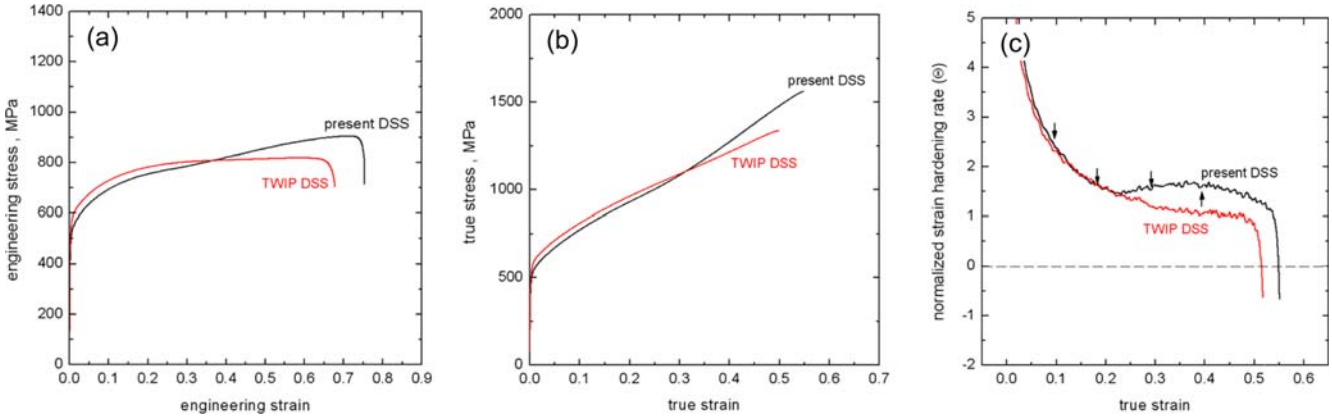

Fig. 2. (a) Engineering stress - strain curves, (b) true stress - strain curves, and (c) normalized strain hardening rate (Θ) - strain (ε) curves of the present DSS and the TWIP DSS: the arrows in (c) indicate the strains where TEM observation was made for the present DSS.

Table 1. Microstructural characteristics and nominal tensile properties of the present DSS and TWIP aided DSS water-quenched after annealing at 1373 K for 5 min: the tensile data are the averages of three runs

	d_A, μm	d_F, μm	f_A	YS, MPa	TS, MPa	e_u, %	e_f, %
present DSS	4.9±1.6	10.0±2.7	0.73	453	900	71	75
TWIP DSS	6.2±1.9	14.6±5.4	0.61	546	819	60	70

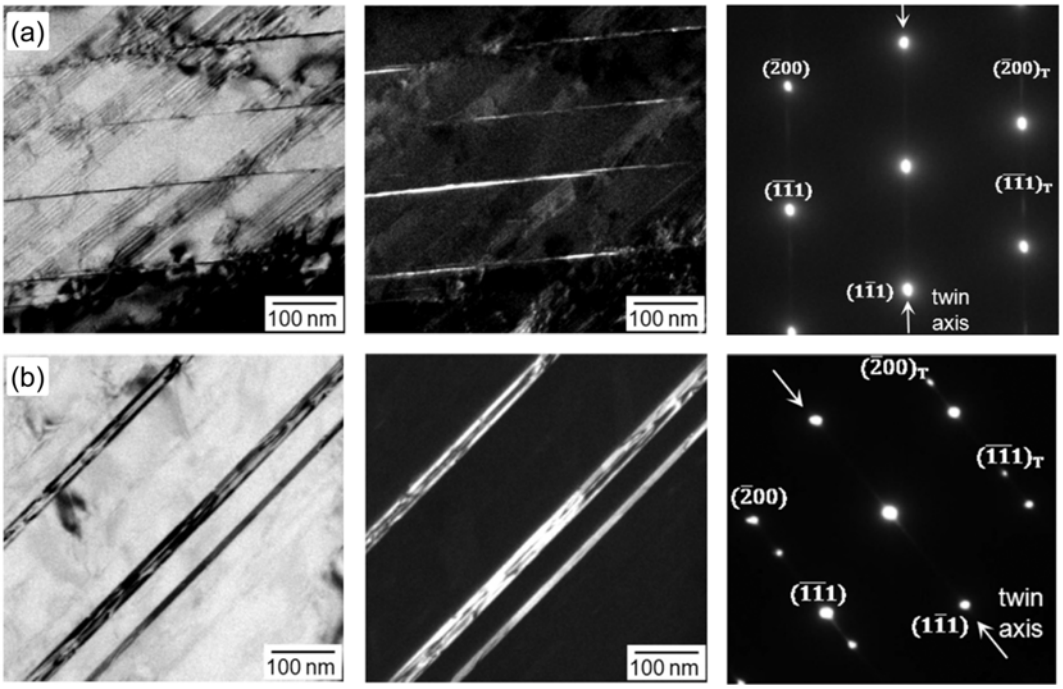

Fig. 3. TEM BF, DF images and SADP ($\underline{z} = [011]_\gamma$) of austenite of the present DSS tensile-deformed with a strain rate of 10^{-3} s^{-1} to (a) ε ~ 0.09 and (b) ε ~ 0.18: DF was taken from the $(\bar{1}\,\bar{1}1)$ twin reflection spot.

Θ of the TWIP aided DSS decreased progressively in the entire strain range. The decreasing rate of Θ of the TWIP aided DSS progressively decreased with strain-, reflecting a deformation sequence of single-variant mechanical twinning → the multi-variant mechanical twinning [10]. Assuming that the contribution of ferrite strain hardening to the overall strain hardening is comparable in the two DSSs, due to the similar ferrite fraction, it is likely that the initial strain hardening of the present DSS was dominated by mechanical twinning (i.e. TWIP) because Θ of the present DSS and the TWIP aided DSS was almost the same up to ε ~ 0.24.

Figures 3a and 3b show the TEM bright field (BF), dark field (DF) images and corresponding selected area diffraction patterns (SADP) of the present DSS deformed to ε ~

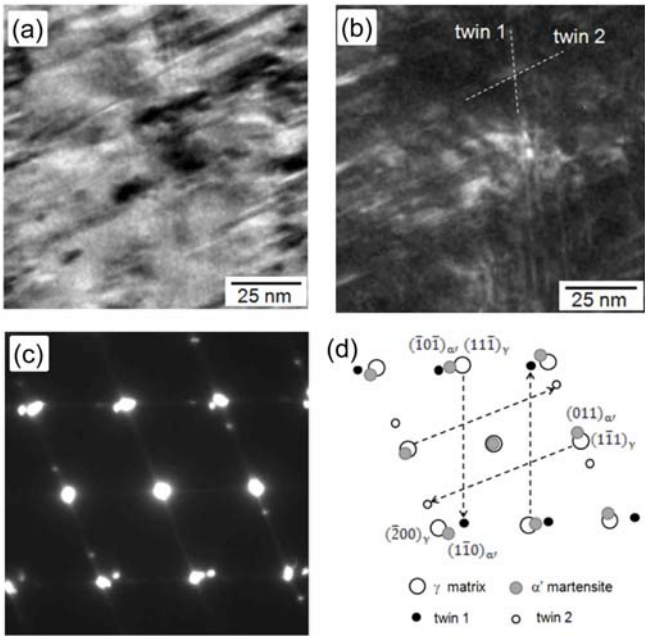

Fig. 4. TEM micrographs of the present DSS tensile-deformed with a strain rate of 10^{-3} s^{-1} to ε ~ 0.28: (a) BF image, (b) DF image, (c) corresponding SADP (z = $[011]_\gamma$//$[111]_{\alpha'}$), and (d) a schematic SADP of (c).

0.09 and ~0.18 respectively: as indicated by the arrows in Fig. 2c, these strains are lower than the strain showing min Θ (ε ~ 0.24). At ε ~ 0.09, thin bands and stacking faults were predominantly observed. SADP (z = $[011]_\gamma$) showing strong austenite spots and weak twin spots diffused along the $[1\bar{1}1]_\gamma$ direction, unambiguously reveals that the thin bands are mechanical twins. At ε ~ 0.18, mechanical twins became thicker and therefore strong twin spots appeared in the SADP. It has been reported that mechanical twinning in austenitic stainless steels has a crystallographic component of {111} <11$\bar{2}$> with the twinning partials of b = 1/6[1$\bar{2}$1] [12]. No ε martensite spots were detected in the SADPs for either strains. Accordingly, as aforementioned, strain hardening of the present DSS up to the stain showing the min Θ (ε ~ 0.24) is associated primarily with TWIP.

Figure 4 shows TEM micrographs of the present DSS deformed to ε ~ 0.28 where Θ increased with strain. The SADP (Fig. 4c) at ε ~ 0.28 is complicated. The SADP analysis (Fig. 4d, z = $[011]_\gamma$//$[111]_{\alpha'}$) reveals the coexistence of double variant mechanical twins (twin 1 and twin 2) and α' martensite. The conjugate of double variant mechanical twins is characterized by an intersection acute angle of 70°. The crystallographic components of double variant mechanical twins with a 70° intersection angle are reported to be $[110]_\gamma$ //$[110]_{twin1}$, $(\bar{1}1\bar{1})_\gamma$//$(\bar{1}11)_{twin1}$ and $[110]_\gamma$//$[110]_{twin2}$, $(\bar{1}11)_\gamma$//$(1\bar{1}1)_{twin2}$ [16,17]. The austenite matrix and α' martensite were found to have the Kurdjumov - Sachs (KS) orientation relationship of $\{111\}_\gamma$//$\{110\}_{\alpha'}$ and $<110>_\gamma$//$<111>_{\alpha'}$. This SADP makes it clear that α' martensite resulted from the SIM transformation at mechanical twin intersections. At this strain, the α' martensite existed in the form of nano-sized islands, as indicated in the TEM BF (Fig. 4a) and DF images (Fig. 4b). Inamura *et al.* [18] also reported the formation of nano-sized SIM islands at the mechanical twin intersections in the surface area of heavily machined austenitic 316 stainless, and they had the KS relationship with austenite matrix with a habit plane of $(2\bar{5}2)_\gamma$. The presence of the nano-sized SIM islands indicates that the Q increase beyond the stain showing the min Θ (i.e. ε ~ 0.24) can be attributed to TRIP.

TEM micrographs of the present DSS deformed to ε ~ 0.41, which is close to the strain showing the peak Θ, are shown in Fig. 5. The BF image (Fig. 5a) reveals the highly deformed state. The DF images taken with the twin reflection of $(111)_\gamma$ (Fig. 5b) and the a' reflection of $(110)_{\alpha'}$ (Fig. 5c) clearly show mechanical twins and SIM. The conjugate twins were not clearly observed at this strain, unlike the microstructures developed at ε ~ 0.28. Because no ε martensite spots were detected at this strain, like the microstructures observed at lower strains, the nucleation and growth of SIM are certainly associated with mechanical twins, although only single-variant twins were observed. The SIM was lath-shaped along mechanical twins. The corresponding SADP analysis (Figs. 5d and 5e, z = $[110]_\gamma$//$[001]_{\alpha'}$) indicates that the SIM in Fig. 5c have the Nishiyama - Wassermann (NW) orientation relationship of $\{111\}_\gamma$//$\{110\}_{\alpha'}$ and $<110>_\gamma$//$<001>_{\alpha'}$ with the austenite matrix. In other areas of the same TEM sample, the KS relationship was also observed.

The SIM transformation at the boundaries between the austenite matrix and the single variant mechanical twins was observed in cold rolled 316 stainless steel by Nakada *et al.* [19]. In such a case, SIM has the KS relationship with both austenite and the mechanical twin, a so-called 'double KS relationship'. They also investigated the SIM transformation behavior in cold drawn 316 stainless steel. In contrast to cold rolling, the cold drawn sample predominantly exhibited the double variant mechanical twins, and the SIM nucleated primarily at the mechanical twin intersections. They concluded that the SIM transformation was more enhanced by cold drawing than by cold rolling since intersections of the double variant mechanical twins provide more SIM nucleation sites.

The present results clearly reveal that the sequential operation of TWIP followed by TRIP associated with SIM nucleation at mechanical twin intersections is beneficial to extend strain hardening to higher strains. As aforementioned, occurrence of TWIP and TRIP depends on the austenite stability. The stacking fault energy (SFE) and M_{d30} temperature are often cited as measures of the austenite stability: the M_{d30} temperature is the temperature at which SIM of 50% is formed at ε = 0.3 [20]. However, the SFE is the measure of ε martensite transformation from austenite rather than α' martensite formation itself responsible for the TRIP effect: ε martensite

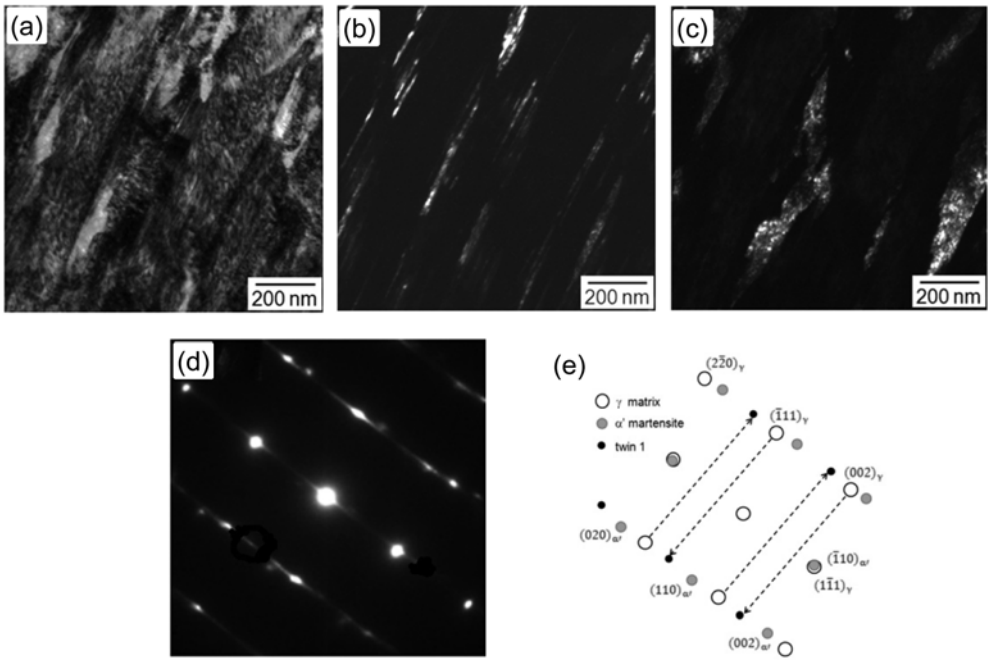

Fig. 5. TEM micrographs of the present DSS tensile-deformed with a strain rate of 10^{-3} s^{-1} to $\varepsilon \sim 0.41$: (a) BF image, (b) DF image taken from the $(\bar{1}11)$ twin reflection spot, (c) DF image taken from the (110) martensite reflection spot, and (d) SADP ($z = [011]_\gamma // [111]_{\alpha'}$), and (d) a schematic SADP of (d).

transformation is favorable at SFE < 20 mJ/m^2 while mechanical twinning is apt to occur at SFE > 20 mJ/m^2 [21]. So, the SFE can be applied when ε martensite appears as an intermediate phase for SIM transformation. Since no ε martensite was detected during deformation of the present DSS, it is appropriate to describe the austenite stability in terms of the M_{d30} temperature. Of several empirical expressions for the M_{d30} temperature in the literature [20,22-24], the following expression by Nohara *et al.* [23] describes the effects of all elements of the present DSS, particularly involving the contribution of Cu equal to that of Ni:

$$M_{d30}\,(°C) = 551 - 462\,(\%C+\%N) - 9.2\,(\%Si) - 8.1\,(\%Mn) - 13.7\,(\%Cr) - 29\,(\%Ni+\%Cu) - 18.5\,(\%Mo) - 68\,(\%Nb) - 1.42\,(GS-8)$$

where the GS is the ASTM grain size number.

For the purpose of comparing of the M_{d30} temperature between the present DSS and TWIP aided DSS, the wt% of elements partitioned in the austenite of the two DSSs was examined by EPMA, as listed in Table 2. In the EPMA measurement, reliable data of carbon and nitrogen were not obtained due to their small bulk amount. However, because the bulk amounts of carbon and nitrogen of two DSSs were almost the same (0.23N-0.05C for the present steel and 0.25N-0.05C for TWIP aided DSS) and the two DSSs were subjected to identical annealing, it can be assumed that the wt% of two elements partitioned to the austenite of the two DSSs is the same.

Table 2. wt% of the substitutional elements partitioned in austenite of the present DSS and TWIP aided DSS water-quenched after annealing at 1373 K for 5 min.

	Cr	Mn	Ni	Cu	Si
present DSS	18.24	3.35	1.35	2.46	0.70
TWIP DSS	18.74	3.94	2.54	2.61	1.44

Under this assumption, the relative M_{d30} difference between the two DSSs can be deduced in terms of the contribution of other substitutional elements and the GS. Along with data in Table 2 and GS ~12, the M_{d30} temperature of the present DSS is ~57 C higher than that of the TWIP aided DSS, indicating that the former is more susceptible to SIM transformation. As addressed by Herrera *et al.* [7], there are two bounds for developing advanced austenite-based steels by controlling the austenite stability. In One, the austenite is unstable so that TRIP occurs at the early plastic deformation stage, and in another, the austenite is relatively stable so that the additional strain hardening mechanism operating at high strain regime operates and plays the more important role of enhancing the overall strain hardening causing better strength and ductility. The sequential operation of TWIP - TRIP observed in this study is representative of the latter.

4. CONCLUSIONS

In summary, the above results provide the following information. (A) The overall strain hardening of the present DSS is

governed by the sequential operation of TWIP followed by TRIP in austenite as deformation proceeds in spite of a considerable fraction of ferrite. (B) In the present case, SIM primarily nucleated at mechanical twin intersections in association with the susceptibility of austenite to SIM transformation, although the austenite was stable enough to suppress SIM transformation at early deformation stage. And (C), the synergetic effects of TWIP and TRIP by their sequential operation is beneficial for extending strain hardening to higher strains compared to the individual operation of TWIP.

ACKNOWLEDGEMENT

This work was supported by POSCO under the contract #2012X011.

REFERENCES

1. Y. T. Shin, H. S. Shin, and H. W. Lee, *Met. Mater. Int.* **18**, 1037 (2012).
2. S. H. Bae and H. W. Lee, *Met. Mater. Int*. **19**, 563 (2013).
3. L. Remy and A. Pineau, *Mater. Sci. Eng. A* **28**, 99 (1977).
4. T. S. Byun, *Acta Mater*. **51**, 3063 (2003).
5. M. Fujisawa, Y. Kato, and T. Ujiro, *CAMP-ISIJ* **21**, 602 (2008).
6. M. Fujisawa, Y. Kato, and T. Ujiro, *CAMP-ISIJ* **22**, 1163 (2009).
7. C. Herrera, D. Ponge, and D. Raabe, *Acta Mater.* **59**, 4653 (2011).
8. J. Y. Choi, J. H. Ji, S. W. Hwang, and K.-T. Park, *Mater. Sci. Eng. A* **534**, 673 (2012).
9. J. Y. Choi, J. H. Ji, S. W. Hwang, and K.-T. Park, *Mater. Sci. Eng. A* **535**, 32 (2012).
10. J. Y. Choi, S. W. Hwang, and K.-T. Park, *Metall. Mater. Trans. A* **44**, 597 (2013).
11. P. L. Mangonon and G. Thomas, *Metall. Trans.* **1**, 1577 (1970).
12. B. Hwang, T. H. Lee, and S. J. Kim, *Phil. Mag. Lett.* **92**, 93 (2012).
13. C. X. Huang, G. Yang, Y. L. Gao, S. D. Wu, and S. X. Li, *J. Mater. Res.* **22**, 724 (2007).
14. J. Y. Choi and W. Jin, *Scripta Mater.* **36**, 99 (1997).
15. R. T. van Tol, J. K. Kim, L. Zhao, J. Sietsma, and B. C. De Cooman, *J. Mater. Sci.* **47**, 4845 (2012).
16. T. H. Lee, C. S. Oh, S. J. Kim, and S. Takaki, *Acta Mater.* **55**, 3649 (2007).
17. T. H. Lee, E. Shin, C. S. Oh, H. Y. Ha, and S. J. Kim, *Acta Mater.* **58**, 3173 (2010).
18. T. Inamura, K. Takashima, and Y. Higo, *Phil. Mag*. **83**, 935 (2003).
19. N. Nakada, H. Ito, Y. Matsuoka, T. Tsuchiyama, and S. Takaki, *Acta Mater*. **58**, 895 (2010).
20. T. Angel, *J. Iron and Steel Inst.* **177**, 165 (1954).
21. G. B. Olson and M. Cohen, *Metall. Trans. A* **7**, 1897 (1976).
22. J. Sjöberg, *J. Wire* **23**, 155 (1973).
23. K. Nohara, Y. Ono, and N. Ohashi, *ISIJ Int.* **63**, 212 (1977).
24. A. Frehn, E. Ratte, and W. Bleck, *Steel Grips (Suppl. High Nitrogen Steels 2004)*, **2**, 447 (2004).